REPORT DOCUMENTATION PAGE

AFRL-SR-BL-TR-01-

0588

1. AGENCY USE ONLY *(Leave blank)*

2. REPORT DATE

3. R

01 JUN 97 to 30 Nov 00 Final

4. TITLE AND SUBTITLE

(AASERT-97) (BMDO) MQW Refractive index modulators for interfacing parallel electronic computers and serial fiber links

5. FUNDING NUMBERS

61103D
3484/TS

6. AUTHOR(S)

Professor Esener

7. PERFORMING ORGANIZATION NAME(S) AND ADDRESS(ES)

University of California San Diego
9500 Gilman Drive
La Jolla, CA 92093-0934

8. PERFORMING ORGANIZATION REPORT NUMBER

9. SPONSORING/MONITORING AGENCY NAME(S) AND ADDRESS(ES)

AFOSR/NE
801 North Randolph Street Rm 732
Arlington, VA 22203-1977

10. SPONSORING/MONITORING AGENCY REPORT NUMBER

F49620-97-1-0388

11. SUPPLEMENTARY NOTES

AIR FORCE OFFICE OF SCIENTIFIC RESEARCH (AFOSR)
NOTICE OF TRANSMITTAL DTIC. THIS TECHNICAL REPORT
HAS BEEN REVIEWED AND IS APPROVED FOR PUBLIC RELEASE
LAW AFR 190-12. DISTRIBUTION IS UNLIMITED.

12a. DISTRIBUTION AVAILABILITY STATEMENT

APPROVAL FOR PUBLIC RELEASED; DISTRIBUTION UNLIMITED

12b. DISTRIBUTION CODE

13. ABSTRACT *(Maximum 200 words)*

During the course of this program, we have developed a measurement setup to measure index of refraction in III-V thin film semiconductors and investigated theoretically and experimentally the refrative index modulation in MQW and DX materials. We have shown that although small in magnitude index modulation exists above absorption saturation. Although we spent considerable effort in growing DX materials we were not able to demonstrate conclusively optical modulation in this type of materials. In this report, we summarize the the refractive index modulation in MQW materials beyond absorption saturation, describe the phase-shift interferometry methods, and detail the measurement results. We also expand on our research on DX center materials.

20011126 096

14. SUBJECT TERMS

15. NUMBER OF PAGES

16. PRICE CODE

17. SECURITY CLASSIFICATION OF REPORT	**18. SECURITY CLASSIFICATION OF THIS PAGE**	**19. SECURITY CLASSIFICATION OF ABSTRACT**	**20. LIMITATION OF ABSTRACT**
UNCLASSIFIED	UNCLASSIFIED	UNCLASSIFIED	UL

Final Technical Report

MQW Refractive Index Modulators For Interfacing Parallel Electronic Computer to Serial Fiber-Links

AASERT Program

Sponsored by

AFOSR Under Grant No. F49620-97-1-03388

Grantee

The Regents of the University of California

University of California, San Diego

La Jolla CA 92093

June 2001

Principal Investigator: Sadik C. Esener
(619) 534-2723

Program Manager: Dr. A. Craig
(202) 767-4934

TABLE OF CONTENTS

List of figures

1. Objectives and Accomplishments

The main objective of this program that was funded in conjunction with the parent program (AFOSR No. F49620-96-1-0309) was the feasibility study for modulating the refractive index in III-V semiconductor multiple-quantum-well (MQW) materials.
This program resulted in one Ph.D. Thesis authored by M. Hansen, entitled "High intensity phase modulation using absorption saturated multiple quantum wells," Ph.D. Dissertation, Electrical Engineering (Applied Physics), UCSD.
Traditionally, thin film III-V devices have been limited to the use of absorption modulation at low optical intensity. Although, the index modulation in MQW material is considerably higher than in other electro-optical materials, this effect is masked by the absorption leading to phase modulated devices with very high insertion loss.
During the course of this program, we have developed a measurement setup to measure index of refraction in III-V thin film semiconductors and investigated theoretically and experimentally the refractive index modulation in MQW and DX materials. We have shown that although small in magnitude index modulation exists above absorption saturation. Although we spent considerable effort in growing DX materials we were not able to demonstrate conclusively optical modulation in this type of materials

In this report, we summarize the the refractive index modulation in MQW materials beyond absorption saturation, describe the phase-shift interferometry method, and detail the measurement results. We also expand on our research on DX center materials.

2. Theoretical Background

The refractive index of a material is the macroscopic representation of light matter interaction when a photon field is passing through a medium. The interaction takes a form of photon absorption and re-emission by atomic dipole oscillators. When there is no energy loss in the passing photon field, the net result of the interaction is a phase delay represented by the refractive index. A permanent energy loss occurs when oscillators are excited to any higher energy states resulting from the absorption of photons. This usually occurs at the oscillator resonant energy. The refractive index is larger near the resonant energy as well because the light matter interaction is strongest at this energy.

The electron energy states are quantized in MQW material, and the resonant conditions occur at each quantized levels. The exciton (spatially bounded electron/hole pair) resonant energies are slightly below each quantized energy level. Corresponding refractive indices are higher near the exciton energy levels and photon absorption occurs at these levels. Thus there are specific energy levels corresponding to exciton oscillators, for which absorption and refraction in a MQW material can be associated with.

Absorption and index are coupled in an absorbing material through the Kronig-Kramers relation. Since the absorption coefficient in MQW material can be modulated electrically through the Quantum-Confined Stark Effect, the density of excitons is thus a function of applied electric field. Since the density of excitons also governs the refractive behavior of the material, the refractive index is also modulated by the electric field.

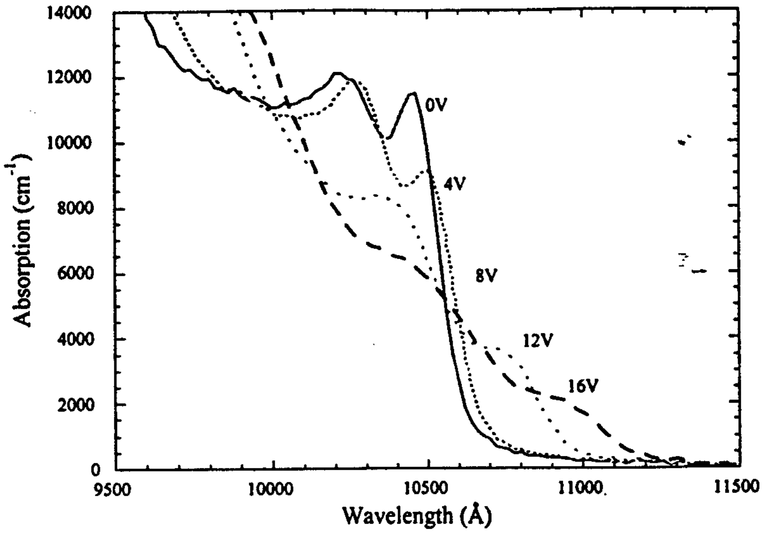

Figure1: Low optical intensity electroabsorption spectrum for InGaAs/InAlGaAs MQWs. Notice the shift of the exciton absorption peak to longer wavelength with applied field. Broadening and reduction of absorption peak height also occur with applied field due to the reduction in electron-hole wavefunction overlap

The absorption coefficient spectra can be measured in function of applied-electric-field conditions. Figure 1 shows measured results in an InGaAs/InAlGaAs MQW material. Refractive indices can be calculated following the classical Kramers-Kronig relation. Figure 2 shows the calculated refractive index from the 0-V curve in Figure 1. Similarly, one can repeat the calculation for each curve in figure 1 and obtain the refractive index spectrum at each field condition. Figure 3 shows the calculated refractive-index spectra. The index modulation can thus be obtained with the applied electric field at a specific optical wavelength. For example, the expected index modulation is –0.01 at the 8-V applied voltage at the wavelength 1.064μm.

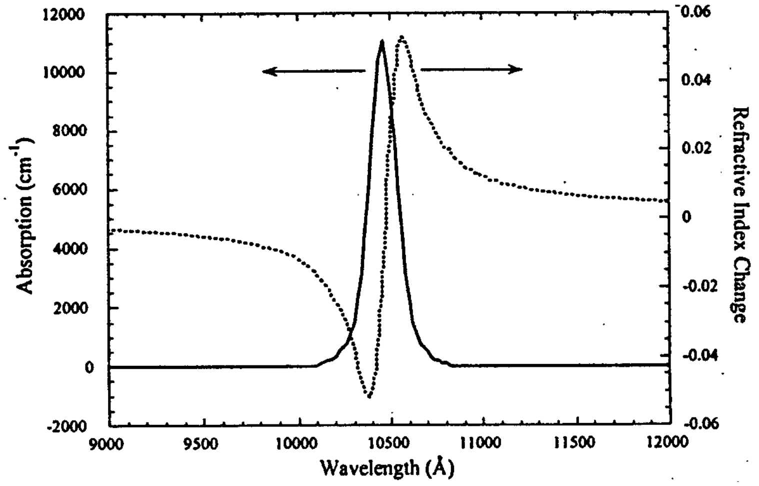

Figure 2: The measured exciton absorption resonance was isolated from the absorption spectrum (solid line), then its effect on the index as an isolated oscillator was estimated via a Kramers-Kronig transform (dashed line).

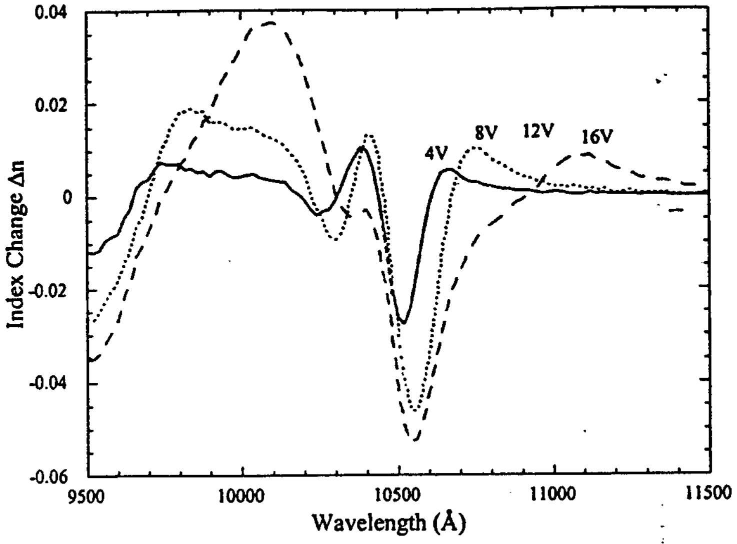

Figure 3: Electro-refraction spectrum estimated from the electro-absorption spectrum through the use of a Kramers-Kronig transform

However, in MQW materials, the exciton absorption can saturate at rather low intensities. It is then interesting to consider the refractive index of a MQW material where the exciton absorption is saturated. After the absorption is saturated, the material behaves more like a dielectric material with a constant refractive index. The value of this constant depends on the nature and the density of the oscillators. The density of exciton oscillators should be at its maximum when absorption is saturated, and the maximum value is a function of the absorption coefficient before the saturation.

Several phenomena occur when the absorption saturates in a material as a result of high concentration of photo-generated particles. They affect the absorption coefficient, the refractive index, and/or the internal electric field. These effects include Bandfilling, Bandgap Renormalization, Thermal Effects, and Electric field screening and can significantly affect the measurement of the refractive index under saturated absortion condition in MQW materials. These effects have been studied in detail in the parent program.

3. Index of refraction measurement

To measure the refractive index modulation above saturation intensity, a method of phase shift interferometry was used. To avoid the thermal effect, a pulse laser with picosecond pulse duration was used in the experiment. The interference fringes were generated by a wedged sample of surface-normal reflection-mode modulator. Interference fringes in the optical window of the MQW modulator were magnified, imaged onto a CCD, and captured by a computer. Then, the phase of the fringe pattern was determined row by row in the image through Fourier analysis. Fringe phases were compared between pairs of images captured with the modulator in the biased and unbiased states.

The change in the index of refraction between these two states could then be calculated from the measured phase change.

3.1 *Sample Preparation*

The material used in these experiments was designed to operate at wavelengths compatible with commonly available high power lasers, such as YAG and YLF lasers, near 1.064μm. InGaAs/InAlGaAs quantum well material can be grown on GaAs wafers to show an exciton resonance at the desired wavelength. For operation at or near 1.06μm, however, the indium concentration in the InGaAs well material must be near 20%. This represents close to a 2% lattice mismatch with respect to the GaAs substrate. Strain relief occurs in the form of dislocations that propagate to the surface, degrading device performance. Buffer layers can mitigate strain effects caused by the lattice mismatch. Such layers are grown underneath the quantum well material to gradually change the lattice constant to that of the well material. As has been demonstrated, the techniques of using linear graded, step graded, and superlattice buffers have been effective in filtering the threading dislocations generated from the lattice mismatch.[12,13] The buffer layers prevent a majority of the threading dislocations from propagating up through the material and into the active device layers.

PIN diode modulators were fabricated in the epitaxial layers on the front surface of the GaAs wafer sample using common lithographic and wet etching techniques. The backside of the sample was mechanically polished with an intentional wedge to generate interference fringes at a particular spatial frequency. Then a high reflectivity (at near-IR wavelengths) gold mirror was thermally evaporated onto the backside of the sample. The result is a reflective mode surface normal MQW modulator with an internal cavity to generate interference fringes.

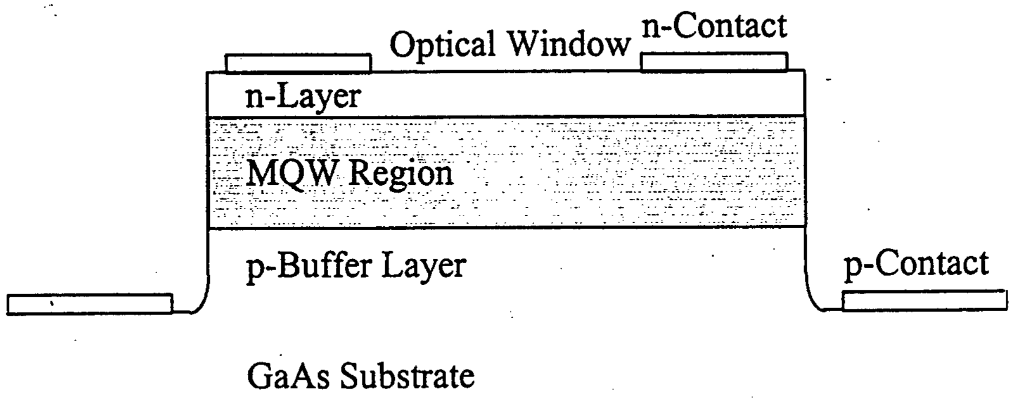

Figure 4: Cross-section view of the PIN modulator

The MQW material was processed into PIN ring diodes, with an optical window in the center of a ring contact. See Figure 4 for a diagram of the diode structure. Wet etch mesa isolation was used to electrically separate the modulators. A common ground plane, the p-doped buffer layers, was used for one electrical contact. The other contact, the n-doped cap layer, was located on top of the mesa. A typical lithographic and wet etching procedure was used to fabricate the devices. Electrical contacts were made using annealed AuGe and CrAuZn metallization.

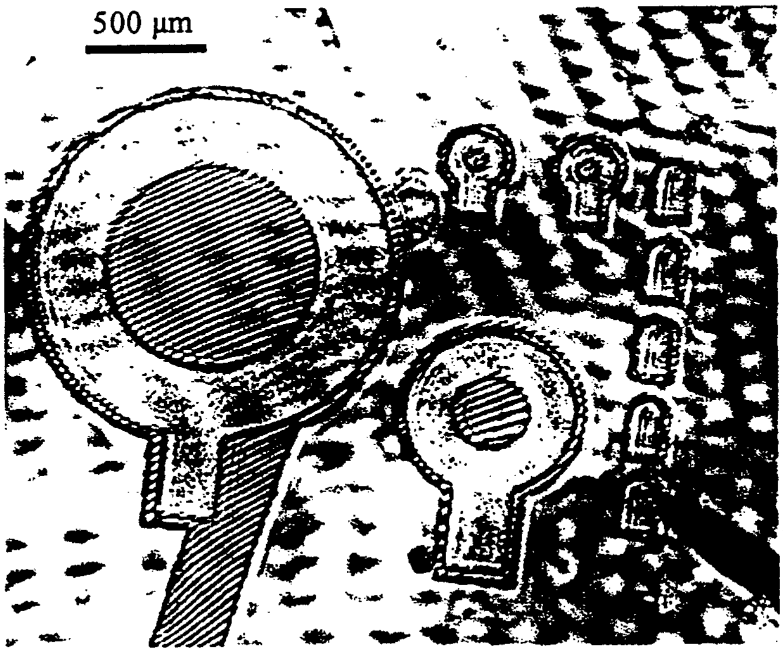

Figure 5: Several sizes of ring diodes fabricated on the InGaAs/InAlGaAs MQW material. Coherent illumination readily shows the straight interference fringes generated in diode windows due to the sample wedge angle. An electrical probe tip is visible at the lower right. The straight bar leading into the large size modulator is a break in the ground plane metallization caused by shadowing of the sample holder clip during the metal evaporation. Interference fringes can be seen in this area as well as the diode windows

The ring diodes were fabricated in several sizes on the sample, as can be seen in Figure 4. This image was formed with coherent illumination at 1064nm. The straight interference fringes due to the wedged sample are easily seen in the ring diode windows. The front surface of the modulator has a reflectivity of roughly 30% from the air-semiconductor interface, which interferes with the light returning from the back reflector. The wedge between the two surfaces generates straight interference fringes when the device is illuminated with coherent light.

The fringe phase determination method, which is described in detail below, requires approximately 10 fringes to obtain an accurate measurement[14]. Therefore an optical window diameter of 275µm, was chosen as a target size for the 10 fringes.

In order to ensure a fringe spacing of 27.5µm to fulfill the 10-fringe requirement, the backside of the sample was polished with a wedge angle of approximately 0.6°. The wedge angle can be derived from the desired fringe spacing (10 fringes per 275µm) and the phase change for one complete fringe (2π). The wedge angle can be found using the relation

$$\theta = \tan^{-1}\left(\frac{N\lambda_f}{x}\right) \tag{1}$$

where $\lambda_f = \lambda_o/n$, λ_o is the free space wavelength of light and n is the index of refraction of the wedge material, x is the total length of the fringes, N is the number of fringes, and θ is the wedge angle as in Figure 6.

The accuracy of the wedge polishing process was optically monitored with the sample mounted on the polishing chuck. Adjustments to the process could then be made with a minimum of handling of the device. After the polishing procedure was completed, a high reflectivity gold mirror was thermally evaporated onto the back surface. Approximately 2000Å of gold was evaporated onto 50Å of chromium used as a sticking layer.

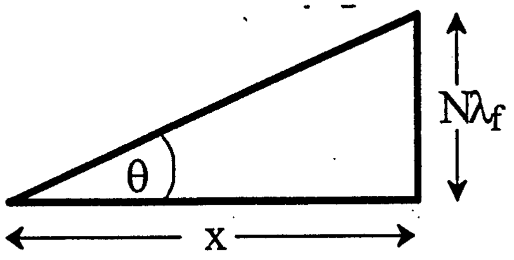

Figure 6: Geometry of an optical wedge

3.2 *Measurements*

Two sets of experiments were taken. First, photocurrent measurements were performed to estimate the saturation intensity for the MQW diodes. Then, a high precision phase shift measurement were made to directly measure the change in index of refraction in the MQW layers under high intensity pulsed operation.

3.2.1 *Photocurrent Measurements*

The measurements were performed under pulsed optical input to determine the saturation power of the MQW modulator under different bias conditions. The photocurrent was monitored as a function of input optical intensity and applied bias. The low intensity linear unsaturated regime and high intensity saturated regimes are clearly delineated.

Using the largest size diode on the MQW sample, window area 0.484 mm^2 (see Figure 4), the current generated from the 10Hz, 35ps laser pulses was measured with a high-resolution ammeter. A Hewlett-Packard Model 3457A digital multimeter with nanoamp resolution was used. The DC current setting of the instrument was used, and the photocurrent generated in the reverse biased diodes from the short laser pulses was enough to register on the ammeter on its most sensitive (nA) scale. By using the DC setting, the value measured is the integrated current over the sampling period of the ammeter. This approach does not quantify the high-speed characteristics of the current pulse, however it does provide a useful measure of photocurrent saturation.

In order to estimate the saturation intensity for the measured photocurrent curves, the data was fitted with a Lorentzian saturation equation, $1/(1+I/I_s)$, in the form of

$$I_{abs}(V) = \frac{I_i k(V)}{1 + \frac{I_i}{I_s(V)}} \qquad (2)$$

where I_i is the incident optical intensity and I_s is the saturation intensity. The $k(V)$ parameter is related to the absorption coefficient at low optical intensity α_o, the absorption length of the modulator material L, and the modulation voltage V through $k(V) = 1-\exp[-\alpha_o(V)L]$.[15]

The measured data is shown in Figure 7 along with fits to the experimental data using Equation (2).

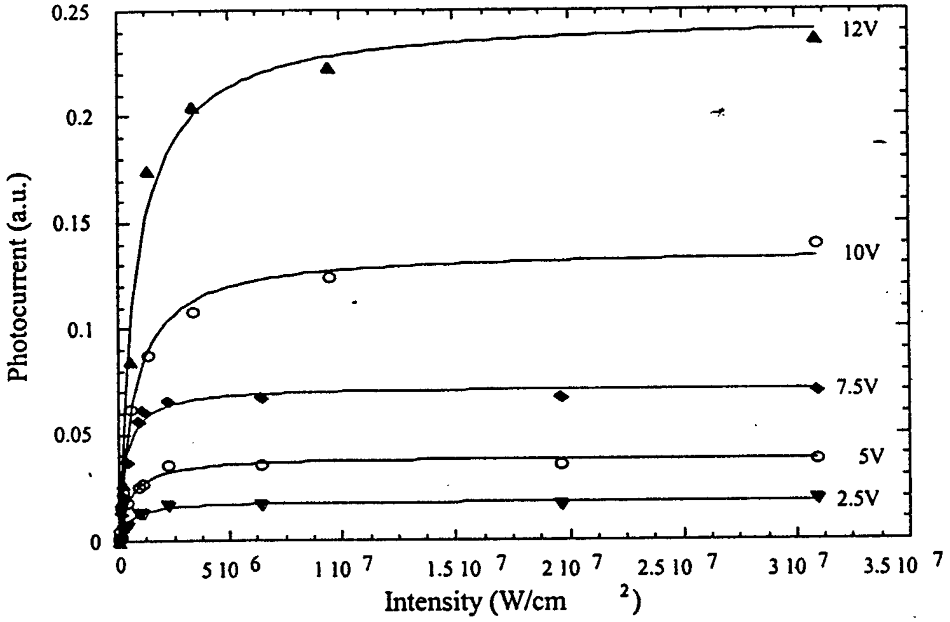

Figure 7: Photocurrent saturation characteristics with pulsed laser input

Table (1) Saturation intensities for optical excitation with 35ps laser pulses

Applied Voltage (V)	k(V)	Is (W/cm^2)
2.5	.088	3.0×10^5
5	.173	4.4×10^5
7.5	.407	4.7×10^5
10	.501	7.0×10^5
12	.653	7.9×10^5

Table 1 lists values for I_s found from the curve fits to the experimental data. Saturation-intensity increasing with applied bias is evident. This suggests faster carrier sweepout from lowered barriers from the electric field. Values of I_s from 100 to 632 kW/cm^2 have been observed by several sources for similar InGaAs/GaAs MQW materials.[12,16] The results presented here are in line with those reported values. These values are considered in the high range for MQW absorption modulators. High saturation intensities can be attributed to fast carrier escape rates and/or fast recombination times. MQW materials with a high density of dislocations from strain relaxation tend to have low quantum efficiencies due to carrier recombination at dislocation sites in the wells. This fast recombination decreases the effective carrier lifetime, so modulators with higher dislocation densities tend to have higher saturation intensities.

3.2.2 Interference Fringe Shift Measurement

To measure the change in index of refraction in the modulator we used fringe shift interferometry method. Fringes result from the reflections of a laser beam from the front and back surfaces of the modulator. The shift of these fringes that result from an applied electric field can reflect a change in index of refraction. The fringes are imaged onto a CCD and are captured with and without an applied electrical bias on the modulator. The phase shift of the interference fringes between the biased and unbiased conditions is then measured with a Fourier analysis of each fringe pattern. The change in index of refraction in the modulator can then be determined once the phase shift is known. Several averaging techniques as well as a simple statistical analysis method were employed to reduce noise and give an estimate of the significance of the results.

Allowing for averaging and statistical analysis techniques, the measurement technique provides for a minimum detectable phase shift on the order of $\lambda/1000$ with a sample size of 50, and $\lambda/2500$ or better with larger sample sizes.

This technique for direct measurement of the change in the index gives the sign as well as the magnitude of the change. It thus yields significant clues to the physics supporting the experiment. This hopefully validates and simplifies the interpretation of the experimental results.

The optical setup used in these experiments was designed with several requirements in mind. The imaging system needed to deliver variable optical power to the diode modulator. The modulators were electrically probed, so a variable magnification system was necessary. The sample is aligned into the system and electrically probed under low magnification. The magnification is then increased so that the fringe pattern in the diode window completely fills the CCD, giving the highest pixel count per complete fringe. A high degree of mechanical stability was also required since the fringe shift measurement is sensitive to vibrations.

The laser used in these experiments was a Continuum PY61C pulsed YAG laser. It generates 35ps pulses at a 10Hz repetition rate. The laser pulse was measured to have a top hat intensity profile. Thus there is a relatively constant intensity across the laser spot, as compared to a typical Gaussian intensity profile.

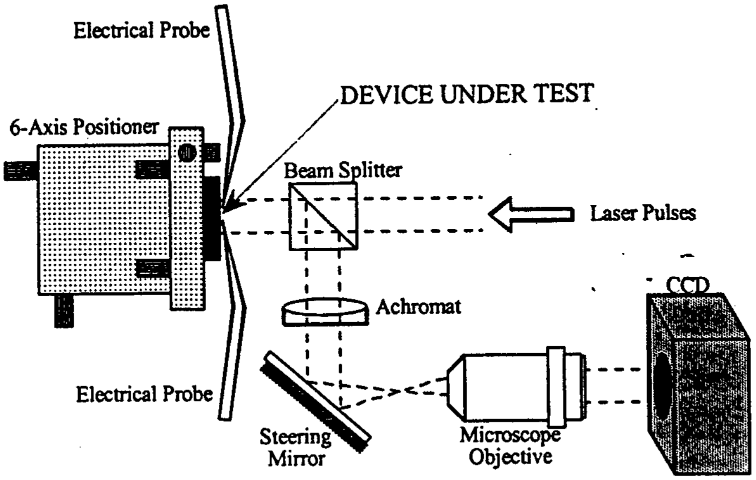

Figure 8: Layout of optical setup used in the precision fringe shift measurement

The camera used to capture the fringe images was a Princeton Instruments Model TE/CCD-1317-K/1. This 16 bit camera uses a cooled CCD, operating temperature of 10°C, with 1316x1034 pixel resolution. The camera is controlled via a Macintosh computer and IPLabSpectrum image processing software from Signal Analytics.

The MQW modulator sample was mounted on a six-axis positioner: XYZ, pitch, yaw, and rotation. The MQW sample was probed electrically using micro-positioners and standard 25μm probe tips. The probes were connected via 50 ohm coaxial cable to a HP E3631A DC variable power supply and a HP 3457A current meter. The current meter was used in this experiment to verify electrical contact had been made with the probes and to monitor the I-V characteristics of the diode before and after the fringe shift experiment.

During the measurement, the modulator sample is flood illuminated with 35ps 10Hz YAG laser pulses. The laser used could provide ample optical power in order to operate the MQW modulator well beyond its continuous wave (CW) absorption saturation point. The YAG laser was used at an average power output of 300mW. With a measured laser spot size of 13.2mm in diameter, this translates into a pulse intensity of $6\text{x}10^8$ W/cm^2. A typical CW saturation intensity for a MQW modulator is on the order of 10^5 W/cm^2, [17] so there is ample optical power available from this laser, even when unfocused. The saturation limit was determined through monitoring of the photocurrent as was described above in the section related to photocurrent measurements.

Each image captured in these experiments represents a 650ms exposure. Thus there are six optical pulses integrated into each image, given the laser's 10Hz rep rate. This multiple pulse integration technique was used to reduce the effects of any intensity variation from pulse to pulse.

Images were captured in groups of 50 via automated image acquisition. Each set of 50 images took approximately 3 minutes to gather. This automated approach was taken to speed data collection in order to reduce error from component drift. Special effort was taken to minimize shifting of the image of the fringes on the CCD due to reasons other than a change in the index of refraction of the sampler. The use of a fast data collection technique proved to be critical in bypassing slowly varying drift components of error. To accurately determine the spatial frequency of the fringes, a one-dimensional FFT was tperformed for each row of a single image. Thus 100 FFTs were performed. As a noise reduction technique the columns of the FFT data were summed. So a one dimensional FFT spectrum was obtained from the summation of the 100 FFTs from the entire image.

To minimize error in the phase calculationdetermination of the spatial frequency should be performed to an accuracy of ±0.1 or better.[47] The FFT function returns values at integer frequency intervals, so an interpolation is performed to find the frequency of the peak in the FFT data when it falls between integer values. In this manner, the spatial frequency of the interference fringe pattern is easily determined to within 0.1.

A profile of the interference fringes generated in the window of the MQW modulator can be written as

$$I_1(x) = W(x)[1 + \cos(2\pi fx - \phi_1)] \tag{3}$$

where x is the spatial coordinate, and f and ϕ_l are the spatial frequency and intrinsic phase of the fringes. The window function of the fringe pattern truncating the signal is represented by W(x). The fringe profile after applying a bias voltage (assuming there is an index change in the well material) can be expressed as

$$I_2(x) = W(x)[1 + \cos(2\pi fx - \phi_1 - \delta\phi)] \tag{4}$$

where the change in phase is represented by $\delta\phi$.

To find the phases of the interference fringes, the Fourier cosine and sine integrals are calculated as

$$C_i = \int_0^1 I_i(x)\cos(2\pi fx)dx$$

$$S_i = \int_0^1 I_i(x)\sin(2\pi fx)dx \qquad (5)$$

where the range of the fringes is normalized and i=1,2. From the Fourier sine and cosine functions the phase of the fringe pattern can be found with the arctangent function:

$$\phi_i = \tan^{-1}(S_i/C_i) \qquad (6)$$

where ϕ_2 is actually $\phi_1+\delta\phi$. Therefore, the phase change can be found as the difference between the phases ϕ_1 and ϕ_2.[18]

There are 100 rows of fringe intensity data in each image captured by the computer. The phase of each row is found using the discrete version of Equation (6):

$$\phi = \tan^{-1}\left(\frac{\sum_x I(x)\sin\left(\frac{2\pi f}{N}x\right)}{\sum_x I(x)\cos\left(\frac{2\pi f}{N}x\right)}\right) \qquad (7)$$

where N is the number of pixels per row and the quantity $2\pi f/N$ is the normalized spatial frequency.

Nakadate[14] used a similar method of analysis to measure phase shifts in a common path interferometer which used Young's fringe generation from a birefringent optical wedge and polarizing filter. He found that, using a CW laser source and a 12 bit resolution image sensor 256 pixels long, the minimum detectable phase shift was λ/4000 and the accuracy was ~λ/2000.

As mentioned previously, the image sensor used in the experiments presented here is a 16 bit resolution 1316x1012 CCD. With 10 complete fringes imaged onto the sensor, there would be 131.6 pixels per fringe. This base resolution, in terms of pixels/fringe, is a factor of five better than in the Nakadate experiments. No averaging techniques were used by Nakadate.

Gathering the data for this experiment, 50 images were saved with the translation stage at its starting position. The translation stage was then stepped 200nm and another 50 images would be acquired. The step and acquire was repeated several times.

After the images were captured for each position of the translation stage, they were processed using the computer to analyze the data. The analysis program reports the phase change of each image in relation to a reference image, which in each case is simply the first image acquired. Plotted in Figure 9 is each phase shift data point. Each point represents the phase of the image relative to the first image acquired, sample number 0. The plot is broken up into sets of 50 images. Listed in Table 2 are the mean values of each of these sets of 50 data points, their standard deviations, and the differences between the means.

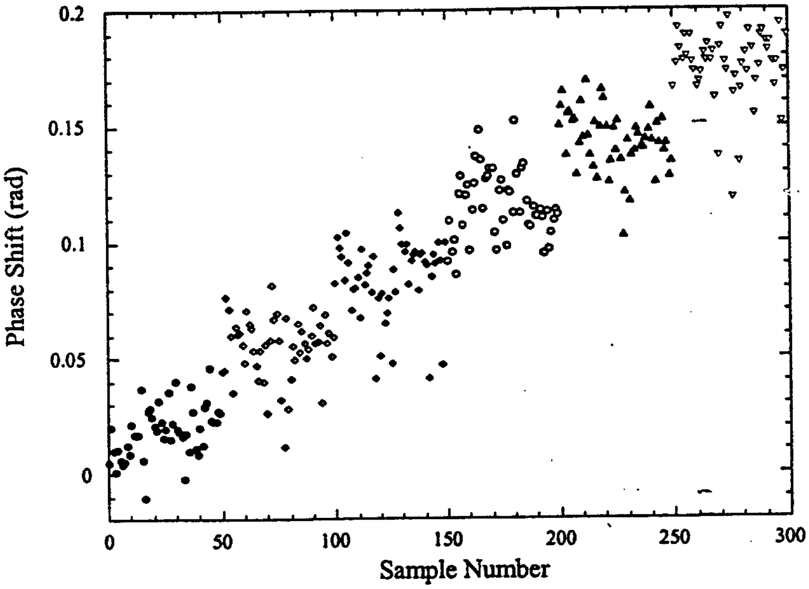

Figure 9:Phase shift data from the verification experiment. Each set of 50 data points were taken with the high-resolution translation stage at a fixed position. The stage was stepped 200nm between each set of data

Table (2). Values of the mean, deviation, and mean difference for each data set presented in Figure (9)

Data Set	Mean	Standard Deviation	Difference of Means
1	0.019	0.0110	
2	0.055	0.0137	0.036
3	0.084	0.0161	0.029
4	0.116	0.0143	0.032
5	0.144	0.0130	0.028
6	0.175	0.0153	0.031

The mean values from Table (2) are plotted in the following figure. The slope of the line fit (and the average of the mean differences) reveals a step size of 0.031 radians which is roughly $\lambda/200$. This compares well with the phase change estimated from the measured fringe spacing of 0.036 radians, a difference of only 16%. The linearity of the measurement is readily apparent from Figure 10.

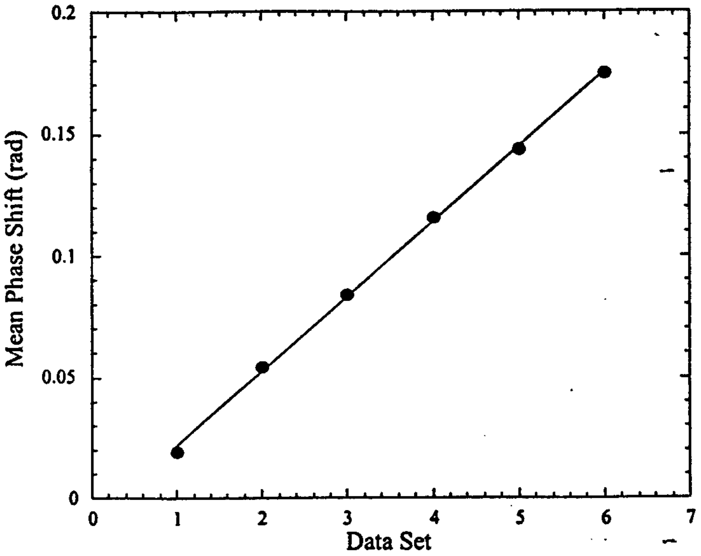

Figure 10: Plot of mean values of each data set of 50 points from Figure (9). A linear fit to the data is also shown

In order to determine the minimum detectable phase change, a common statistical analysis was performed on the data, the T-test. The primary purpose of the T-test is to determine whether the means of two groups of data differ to a statistically significant degree. Two data sets with different means may come from different groups of data, or the observed differences may have occurred by chance or sampling error.[19] The T-test helps determine which is the case.

A T-test is a test is, based on the means, standard deviations, and sample sizes of two data sets, returns a value which indicates the probability that the two samples are likely to have come from the same underlying population[20]. The function used in this evaluation returns a value of 1 if the two data sets are identical, and returns a value of 0 if the data set means are widely separated with small standard deviations. Values between 0 and 1 are returned for data sets whose means are close or that have large deviations.

A two-tailed T-test analysis assuming homogeneous variances was performed on two sets of 50 data points from Figure 9. The analysis was done in a spreadsheet application on a personal computer. The minimum detectable phase change was estimated by finding the separation of the means at which the T-test returned a value of 0.05. This indicates that there is a 95% probability that the two samples come from different populations, or a 5% probability that they come from the same population. The mean of one sample was brought closer to the mean of the other sample through addition of a constant to each data point in the set.

These tests reveal that the 95% confidence level is reached at a mean separation of .0062 radians, or λ/1021. So, with a sample size of 50 data points for each set, the resolution of the system is about λ/1000.

4. Experimental Results

From the phase shift interferometry measurement, groups of 50 data points were recorded for the biased and unbiased conditions. The input biases range from 2 to 12V. In the plot below (Figure 11), data points are presented for the unbiased (0V) state, the solid circles, and the biased (3V) state, the open circles. The input intensity is 1.4x10^7 W/cm^2, nearly two orders of magnitude higher than the measured traditional saturation intensity of 3x10^5W/cm^2 (for a 2.5V bias).

A T-test analysis was performed on adjacent data groups. That is, groups one and two were tested, two and three, etc.. The results of this analysis are presented in Figure 12. Except for the tests 14 and 17 (for data groups 14/15 and 17/18), which do not indicate a significant difference, other seven tests show an 80% or higher confidence level. The average of all the (1 - T-test) values is 0.62.

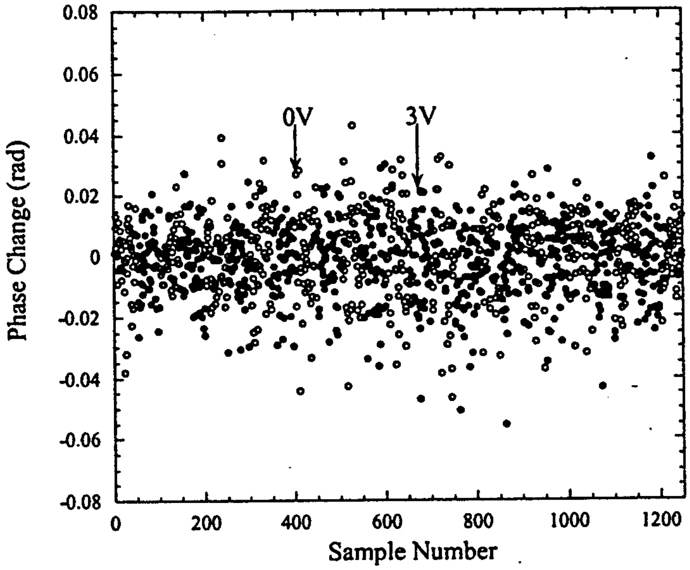

Figure 11: Phase shift data for 0V (closed circle) and 3V (open circle) bias. Data was collected in-groups of 50 for each bias condition, with 13 sets of 0V and 12 sets of 3V bias data being collected

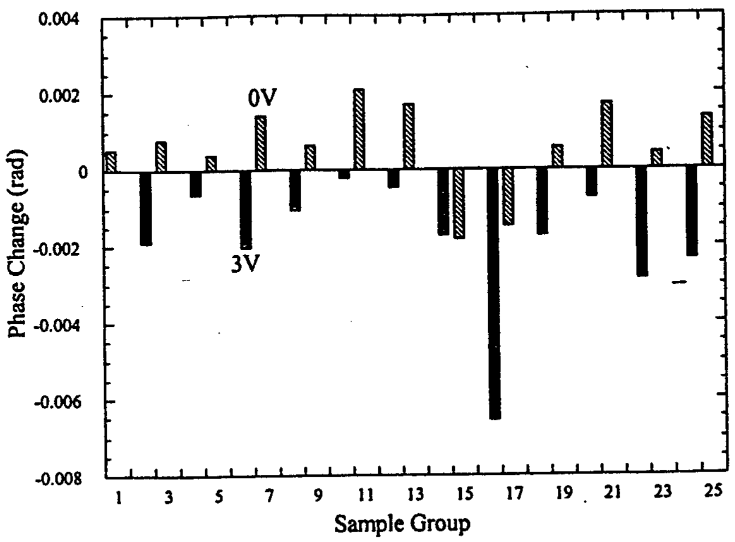

Figure 12: Mean for the groups of 50 data points presented in the previous figure. The solid bars represent the mean values for the biased states (3V) while the striped bars represent the unbiased state (0V)

As a further analysis of the data, the 0V means were separated from the 3V means. The mean of the means was then found for both bias states. This result is most simply presented (Figure 14) as two data points, with error bars representing the standard deviation of the mean of the means calculation. It is evident that there is indeed a measured shift in the phase of the interference fringe pattern. The difference in these values is found to be -0.0025 rad.

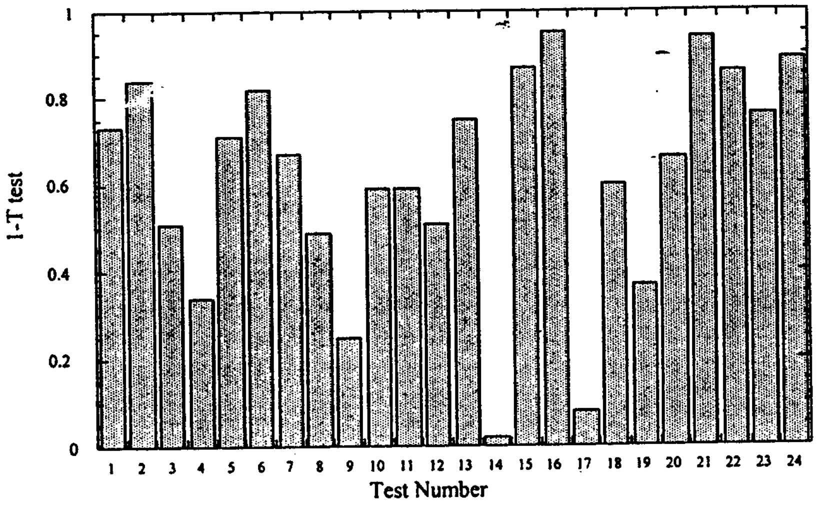

Figure 13: Results of a T-Test analysis on adjacent groups of phase change data. The value of (1-T-test) represents the probability that the two sets of data points come from different populations

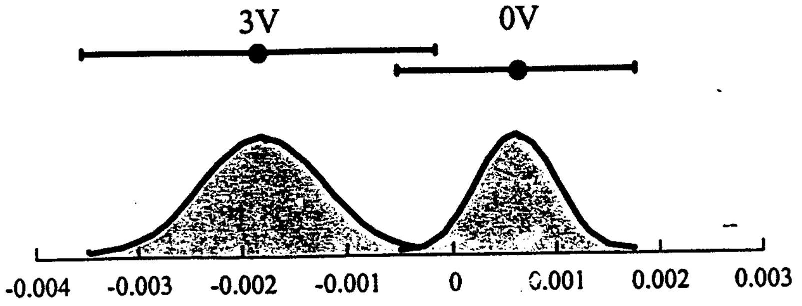

Figure 14: The mean of the means was computed for both the unbiased and biased state. Error bars represent the standard deviation. Gaussian curves representing normal distributions are included as an aid to the eye

The change in the refractive index can be calculated from the change in phase using by

$$\Delta\phi = 2\pi \frac{\Delta n L}{\lambda} \tag{8}$$

where L is the optical path length in the material thickness and λ is the wavelength of light. For a reflective modulator, the optical path length is double of the material thickness. From the measured phase shift $\Delta\phi$ of -0.0025 rad, the change in index is then -4.7×10^{-4}, using L=0.9μm and λ=1.064μm,

Compared to the calculated change in refractive index using Kramers-Kronig relation, Figure 15 (a) and (b), the measured change in refractive index is an order of magnitude smaller. One possible cause is the electric field screening in the modulator under high illumination. The data collected in the fringe-shift measurement for voltages higher than 3V do not show a statistically significant signal, within the experimental resolution. This

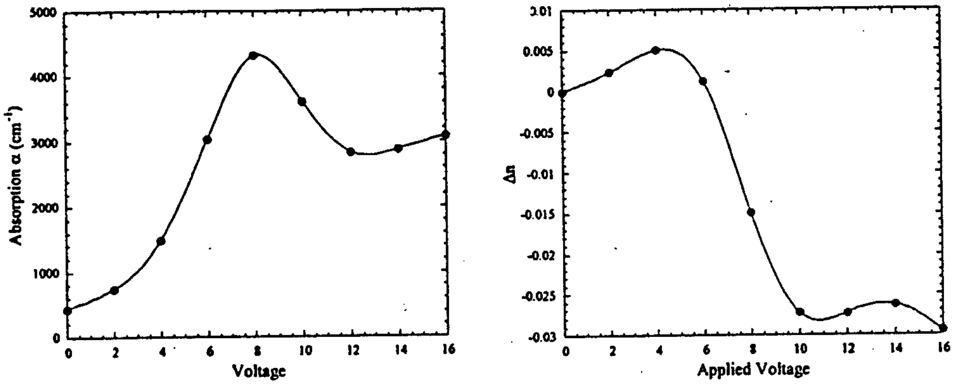

(a) (b)

Figure 15: (a) Absorption and (b) index change for InGaAs/GaAs MQW modulators under low intensity illumination at 1064nm

is an indication of electric field screening. Unfortunately, due to the lack of tunable pulse laser of high power, the detailed dynamic behavior of the absorption and index of refraction could not be investigated.

5. DX Center materials

In this section, we report on our attempt to obtain refractive index modulation in III-V compound semiconductor thin films that incorporated DX centers.

DX centers are point defects observed in n-type doped III-V compound semiconductors. They significantly reduce the carrier concentration and cause persistent photoconductivity (PPC) at low temperature [21,22]. Figure 16 shows the two stable configurations of doping atom, e.g. Si, in III-V compound semiconductors. In $Al_xGa_{1-x}As$ DX state is the ground state of donor atom when $x \geq 0.22$. Depending on the composition and the sample temperature the donor atom in its normal substitutional site (Figure16-a) relaxes into the DX center configuration (Figure16-b) by capturing two electrons from conduction band (CB). As a result of this relaxation a bond between doping atom and one of its As neighbors is broken.

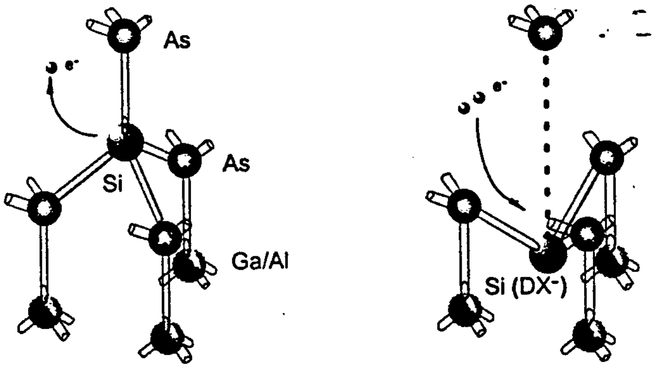

(a) (b)

Figure 16: Two stable configuration of Si atom in III-V compounds. (a) Si atom in substitutional site, and (b) Si atom in DX center configuration. Si atom captures two electrons from conduction band when it moves to DX center configuration

The corresponding energy of these two states can be represented in a configuration diagram as shown in Figure 17. In a configuration diagram total energy, electronics and lattice, of doping atom versus configuration coordinate is plotted. In the diagram shown in Figure 17 the left curve represent the normal substitutional configuration and right curve represents the DX center state, respectively. The thermal capture energy, E_{cap}, is important to understand the PPC effect at low temperature. It prevents equilibrium being established below a critical temperature. When the electrons are optically excited from DX centers into the CB at low temperature they stay in CB because the electrons do not have enough thermal energy to overcome the capture barrier, hence PPC effect. The persistence time of the electrons in CB depends exponentially on the temperature and the height of the capture barrier.

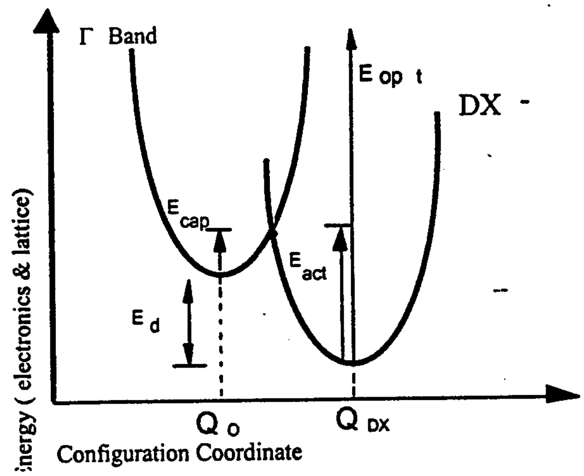

Figure 17: Configuration diagram showing total energy (electronics and lattice) versus configuration coordinate. When Si atom captures two electrons from conduction band (CB) the lattice relaxation takes place and Si atom moves to a distorted position Q_{DX}.

As a consequence of the PPC effect the carrier concentration in CB increases in the order of magnitude. This large change in carrier concentration affects the optical properties of the material. The expected index change due to the increase in free carrier concentration can be estimated by means of plasma effect. The dielectric constant, ε(ω), of a semiconductor is given by

$$\varepsilon(\omega) = \varepsilon_0(\omega) - \frac{\omega_p^2}{\omega^2} \tag{9}$$

where ω is the read-out beam frequency, and ω_p is the plasma resonance frequency and given by

$$\omega_p = \frac{4\pi N e^2}{m^*} \tag{10}$$

Here m* is the effective mass of electron in CB, and N is the free carrier concentration. The expression for the change in refractive index as a function of the net change in carrier concentration ΔN can be expressed as follows [3].

$$\Delta n \cong -\frac{2\pi(\Delta N)e^2}{n_0 m^* \omega^2} \tag{11}$$

where n_0 is the refractive index in absence of free carriers.

In this work we studied DX centers in a Si doped $Al_{0.30}Ga_{0.70}As$ material grown by molecular beam epitaxy (MBE) for a potential use in index modulation. In this material large persistent photoconductivity ($\Delta N = 2.1 \times 10^{18}$ cm^{-3}) is observed. We measured the

anisotropy of the sample resistivity ($R_{\perp}/R_{//} > 10^4$) resulted from modulation of the free carrier density by optical excitation in striped pattern.
The sample studied in this work is a 1 µm thick Si doped $Al_{0.30}Ga_{0.70}As$ grown by molecular beam epitaxy (MBE) on a semi-insulating GaAs substrate. An additional 1 µm undoped $Al_{0.30}Ga_{0.70}As$ layer is also grown between substrate and doped $Al_{0.30}Ga_{0.70}As$ layer to prevent quantum well formation between GaAlAs and GaAs interface. After the growth the sample is cut into a 5x5 mm sample size to do electrical measurement in a van der Pauw geometry. Ohmic contacts are made to the sample with In. -
Figure 18 shows the measured PPC data. In this measurement the sample is cooled down from room temperature to 25 °K in the dark. At 25 °K it is uniformly illuminated with a white light source 20 minutes to excite all the DX centers. After the light is turned off, we waited an additional 10 minutes to make sure that the sample has reached a steady state. The carrier concentration is then remeasured. The net change in carrier concentration below 77 °K is around $\Delta N=2.1\times10^{18}$ cm^{-3}. This increment in carrier concentration is persistent as long as the temperature is kept below the critical temperature, which is 120 °K for GaAlAs based materials.

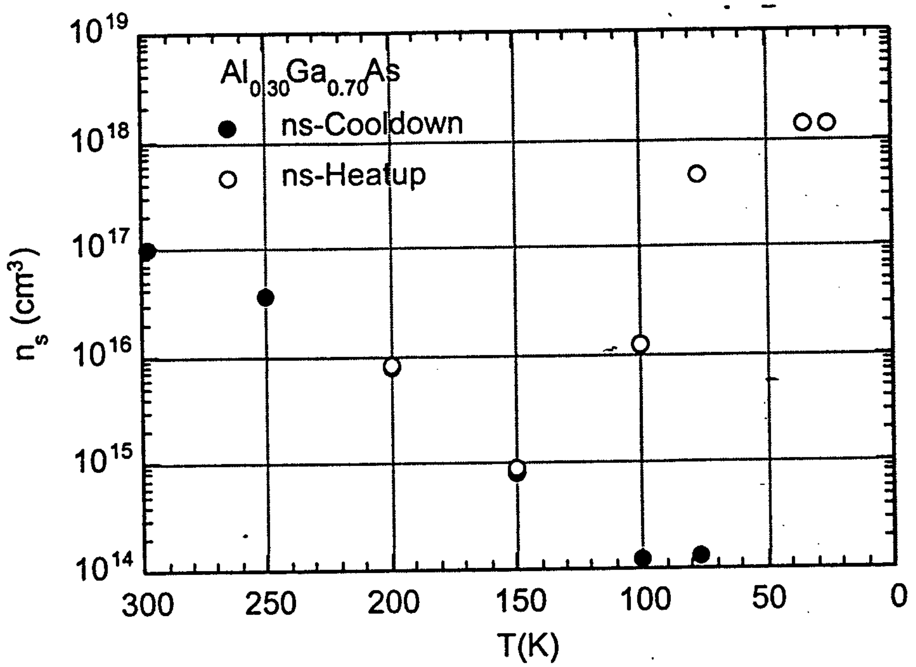

Figure 18: The persistent photoconductivity (PPC) curve for $Al_{0.30}Ga_{0.70}As$:Si. The sample is cooled down from room temperature to 25 °K. At 25 K it is uniformly illuminated 20 minutes with a white light source to excite all the DX centers.

As mentioned above the modulation of the carrier density leads to large refractive index change as a result of the plasma effect. The local nature of the DX centers can be exploited by illuminating the sample with a striped pattern parallel to one of the sample edges. The illuminated portion of the sample will have larger carrier concentration than that of dark region. The difference in the refractive index due to this spatial charge modulation between these two regions can be estimated by using eqs. (11).

Figure 19 shows the experimental setup used to measure such index change. The sample is placed in an optical cryostat which allows us to do low temperature optical and electrical measurements. In this experiment a striped pattern in different grating periods is placed in front of the sample. The sample is illuminated with a HeNe laser (λ=6328 Å) which has enough optical energy to excite electrons from DX centers. This optical illumination in a striped pattern creates modulation of the free carriers along the side of the sample. The sample conductivity is measured along perpendicular ($R_\perp$) and parallel ($R_{//}$) directions using a van der Pauw geometry.

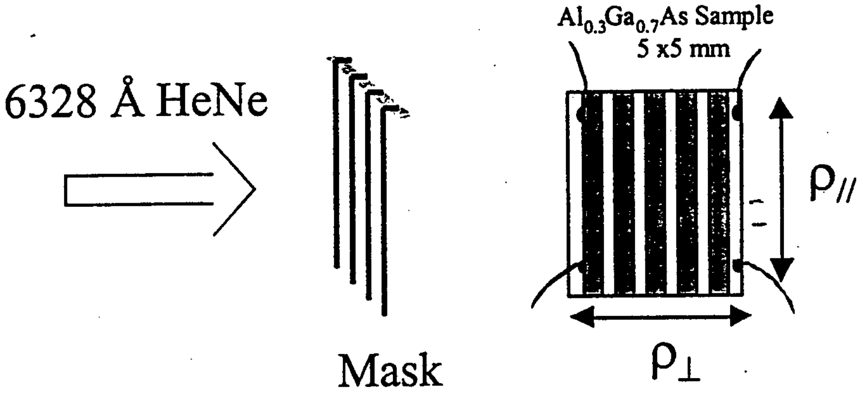

Figure 19: Experimental setup used to measure the modulation of the carrier density. The sample is illuminated with a HeNe laser using a striped pattern parallel to one of the sample edges.

The measured resistivity in perpendicular and parallel directions as a function of grating space is shown in Figure 20. This figure also shows the magnitude of the resistivity anisotropy. When the sample is uniformly illuminated no anisotropy in conductivity is observed. However, if the sample is illuminated with a striped pattern parallel to one of the sample edges a large anisotropy in resistivity, up to 10^4, is observed. It is possible to measure the effect of this charge modulation optically in our setup with a slight modification. Linke et al. optically measured a refractive index change $\Delta n=1.2\times10^{-2}$ in an $Al_{0.29}Ga_{0.31}As$:Si sample doped to a value of 4.0×10^{18} cm^{-3} [24].

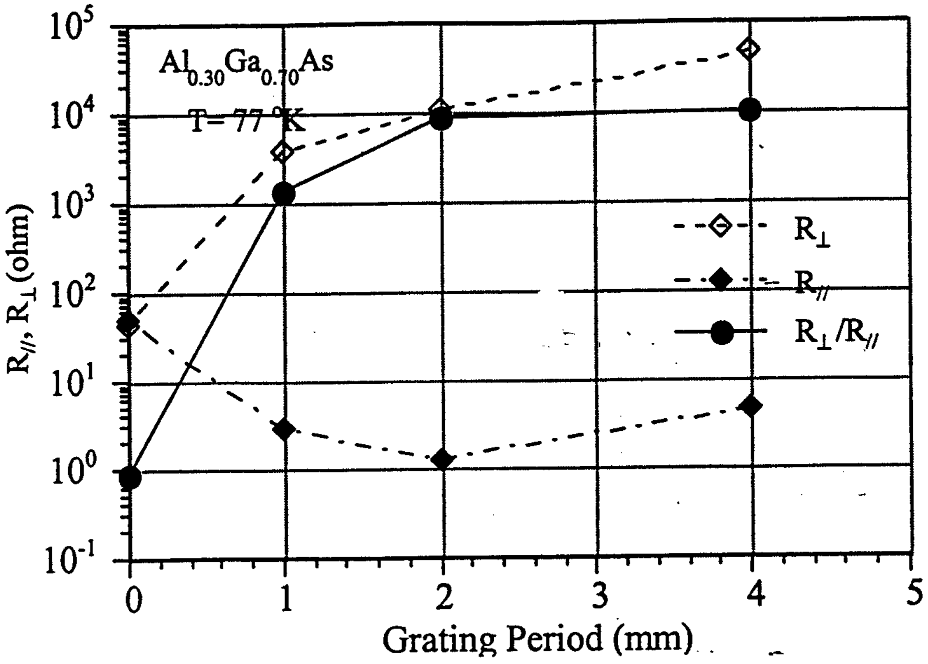

Figure 20: Modulation of the resistivity in $Al_{0.30}Ga_{0.70}As$ as a function of grating period. There is no anisotropy in resistivity when the sample is uniformly illuminated. The anisotropy in resistivity up to $R_\perp/R_{//} > 10^4$ is measured for large grating size.

6. Conclusions

We have demonstrated experimentally the refractive index modulation in MQW materials beyond the absorption saturation. The measured index change at high optical illumination is an order of magnitude smaller than estimated from the low-intensity absorption coefficient, which may indicate the presence of electric field screening under the high-intensity illumination.

As discussed in Section 2, the electric field screening is caused by the unbalanced escaped rates of electrons and holes in the wells. In general electrons are lighter than holes in any material, the screening is more likely caused by holes left in the wells. Therefore, the materials with higher potential barrier for electrons, such as GaAs related component materials, are better suited for the devices operating at high intensity. It has been reported that the incorporation of Nitrides in III-V semiconductor materials results in the increasing of conduction-band offsets in the MQW materials. Further research could be conducted in Nitride related materials if the MQW devices are to be used to modulate phase under high-intensity illumination.

Finally, the phase-shift interferometry method developed during the course of this work is proved to be a high-resolution technique to determine the index change in a material. It has the resolution of λ/2500.

Due to the local nature and PPC effect the DX centers based index modulation could be important for optical devices. The refraction index of the material that contains DX centers can in principle be modulated by excitation of these defects. In this work we measured the spatial modulation of the carrier concentration in $Al_{0.30}Ga_{0.70}As$ material and observed a large anisotropy in conductivity ($R_{\perp}/R_{//} > 10^4$) at 77K.

Although we have tried to measure the refractive index of our materials with the above-described set-up, we were not able to demonstrate any optical modulation in our DX materials. We suspect that due to the small thickness of our films the phase retardation was too small for our set-up to sense. Further studies are needed in this area.

7. References

[1] B. R. Bennett, R. Soref, and J. Del Alamo, "Carrier-induced change in refractive index of InP, GaAs, and InGaAsP," IEEE Journal of Quantum Electronics, Vol. 26, No. 1, 1990, pp. 113-122

[2] A. Yariv, *Optical Electronics*, 3rd Ed. New York: Holt, Rinehart and Winston, 1985, pp. 474-478

[3] N. Peyghambarian, S. Koch, and A. Mysyrowicz, *Introduction to Semiconductor Optics*, New Jersey: Prentice Hall, 1993, p. 331

[4] G. Boyd, J. Cavaillès, L. Chirovsky, and D. Miller, "Wavelength dependence of saturation and thermal effects in multiple quantum well modulators," Applied Physics Letters, Vol. 63, No. 13, 1993, pp. 1715-1717

[5] T. Sizer, R. LaMarche, and T. Woodward, "Point source heating effects in multiple quantum well modulators," Applied Physics Letters, Vol. 61, No. 4, 1992, pp. 420-422

[6] R. Mottahedeh, G. Parry, M. Whitehead, J. Roberts, and C. Button, "High power performance of asymmetric Fabry-Perot MQW modulators," IEEE Photonics Technology Letters, Vol. 6, No. 6, 1994, pp. 703-705

[7] D. Hutchings, C. Park, A. Miller, "Modeling of cross-well carrier transport in a multiple quantum well modulator," Applied Physics Letters, Vol. 59, No. 23, 1991, pp. 3009-3011

[8] A. Fox, D. Miller, G. Livescu, J. Cunningham, J. Henry, and W. Jan, "Exciton saturation in electrically biased quantum wells," Applied Physics Letters, Vol. 57, No. 22, 1990, pp. 2315-2317

[9] T. Wood, J. Pastalan, C. Burrus, B. Johnson, B. Miller, J. deMiguel, U. Koren, and M. Young, "Electric field screening by photogenerated holes in multiple quantum wells: A new mechanism for absorption saturation," Applied Physics Letters, Vol. 57, No. 11, 1990, pp. 1081-1083

[10] M. Watson, J. Chilla, J. Rocca, J. Kim, D. Lile, T. Vogt, and G. Robinson, "Saturation intensity and time response of InGaAs-InGaP MQW optical modulators," IEEE Journal of Quantum Electronics, Vol. 31, No. 2, 1995, pp. 254-260

[11] R. Morgan, L. Chirovsky, M. Focht, R. Leibenguth, "High-power quantum well modulators exploiting resonant tunneling," Applied Physics Letters, Vol. 59, No. 27, 1991, pp. 3524-3526.

[12] T. Woodward, T. Sizer, D. Sivco, and A. Cho, "InGaAs/GaAs multiple quantum well modulators for the 1.02-1.07μm wavelength range," Applied Physics Letters, Vol. 57, 1990, p.548-550

[13] T. Sizer, T. Woodward, U. Keller, K. Sauer, T. Chiu, D. Sivco, A. Cho, "Measurement of carrier escape rates, exciton saturation intensity, and saturation density in electrically biased multiple quantum well modulators," IEEE Journal of Quantum Electronics, Vol. 30, No. 2, 1994, pp. 399-407

[14] S. Nakadate, "Phase detection of equidistant fringes for highly sensitive optical sensing. I. Principle and error analyses," Journal of the Optical Society of America A (Optics and Image Science), Vol. 5, No. 8, 1988. p.1258-1264

[15] C. Fan, B. Mansoorian, D. Van Blerkom, M. Hansen, V. Ozguz, S. Esener, and G. Marsden, " Digital free-space optical interconnections: a comparison of transmitter technologies," Applied Optics, Vol. 34, No. 17, 1995, pp. 3103-3115

[16] K. Goosen, J. Cunningham, M. Santos, and W. Jan, "Measurement of modulation saturation intensity in strain-balanced undefected InGaAs/GaAsP modulators operating at 1.064μm," Applied Physics Letters, Vol. 63, No. 4, 1993, pp. 515-517

[17] C. Barron, C. Mahon, B. Thibeault, G. Wang, W. Jiang, L. Coldren, and J. Bowers, "Milimeter-wave asymmetricFabry-Perot modulators," IEEE Jooumal of Quantum Electronics, Vol. 31, No. 8, 1995, pp 1484-1493

[18] S. Nakadate, "High precision retardation measurement using phase detection of Young's fringes," Applied Optics, Vol. 29, No. 2, 1990, pp.242-246

[19] G. Kranzler, J. Moursund, *Statistics for the Terrified*, New Jersey: Prentice Hall, 1995

[20] B. Brown, M. Hollander, *Statistics: A Biomedical Introduction*, New York: Wiley, 1977

[21]. D. V. Lang, R. A. Logan, and M. Jaros, Phys. Rev. B 19, 1015(1979).

[22]. P. M. Mooney, J. Appl. Phys. 67, R1(1990).

[23]. R. A. Linke, Tineke Thio, J. D. Chadi, and G. E. Devlin, Appl. Phys. Lett. 65, 16(1994).

[24]. R. A. Linke, T. Thio, and J. D. Chadi, J. Appl. Phys. 83, 661(1998).